Distributed motion sensing on ships

Hans-Martin Heyn, Guttorm Udjus, Roger Skjetne
Centre for Autonomous Marine Operations and Systems
Department of Marine Technology
Norwegian University of Science and Technology
7491 Trondheim, Norway
martin.heyn@ntnu.no

***Abstract*—A current trend is autonomous transport of goods and people in the air, at land, and at sea. For safe and reliable operations, autonomous systems require sensors that replace, or even exceed, the senses of a human operator. A system of spatially distributed inertial measurement units (IMUs) along the hull of a vessel, which allows sensing of local accelerations of a vessel or structure at sea is proposed. In contrast to classic motion sensors on ships, the sensors are not placed in a central location of the ship, but are instead mounted on the inside of hull of the vessel. This enables the system to measure local hull vibrations, which are induced by external forces or pressure gradients. The measurements can be processed to allow a spatial awareness of environmental loads or force fields acting on the vessel. After a discussion of the fundamentals of local motion sensing on a marine vessel, this paper presents two applications for distributed motion sensing. The first application is the measurement and classification of ice-induced vibrations in the hull of an Oden-class icebreaker during transit and stationkeeping in ice-infested waters. At four locations on the vessel, the local vibrations were measured and probability distribution function fitted to the motion data. It is shown, depending on the ice-conditions, that the stochastic properties of the signal change. In a second application, a model scale ship is equipped with an array of four motion sensors along the hull of the vessel and one virtual sensor in the center of gravity as a reference measurement. By this configuration, it is demonstrated how to detect local pressure zones along the hull caused by incoming waves.**

Keywords— Arctic, Marine technology, Maximum likelihood estimation, Motion estimation, Sensor arrays, Statistical analysis

I. INTRODUCTION

Distributed motion sensing is an extension of the classical one point motion sensing on ships. Today, many ships are equipped with inertial measurement units (IMUs), placed at a central location in the vessel, typically in an instrument room, as part of an integrated inertial navigation system (INS), which provides, in combination with a global navigation satellite system (GNSS) information about the position, velocity, and attitude of the vessel [1], and sometimes also the corresponding accelerations [2]. An extension of a single motion sensor INS to a system with a triple redundant sensor package is presented in [3]. Besides for navigation purposes, data from a motion sensor on a vessel can also be used for the detection of dangerous operation conditions. One such condition is the occurrence of parametric roll on a vessel. Galeazzi et al. describe in [4] a method for parametric roll monitoring based on the detection of changes in the stochastic properties of the roll motion signal from an onboard IMU. Johnston et al. showed that acceleration data obtained from an IMU in the center of gravity of a ship can also be utilized to determine the global load from interaction with sea-ice [5]. The authors extended their approach with a second IMU, placed in the bow of the vessel, close to the ice interaction zone [6]. They proofed that, for measuring global ice loads, the IMU can be placed arbitrarily inside the ship (given the rigid body assumption). By fusing the acceleration data from a set of four spatially distributed IMU sensors, Kjerstad et al. [7] were able to obtain a full state estimate of the acting accelerations on a vessel. They used the reconstructed acceleration vector as feedforward in a control law to rapidly compensate ice loads. Amongst others, they demonstrated the effectiveness of a spatially distributed sensor setup for dynamic positioning (DP) control in ice infested waters.

All of these application for IMU sensors on ships have the aim of measuring or estimating the global accelerations or global loads acting on the vessel, typically based on rigid body dynamics. Locally occurring motions and vibrations are neglected or actively filtered out of the signal. However, the rigid body assumption is crude, and especially when operating in harsh environments, like ice-infested waters or in large waves, the flexibilities in the ship hull becomes very distinct. Hence, accelerations measured at different locations will not be the same. The analysis of locally induced vibrations thus provides information about the external loads, e.g. the attacking sea-ice [8]. Strain-gauges along the hull of the bow of a vessel provide information about the local load distribution along the hull during ship-ice interaction [9]. This provides spatial knowledge about the ice conditions around the vessel, which can, according to the authors, be utilized in decision supports systems for the crew. The measurement of locally induced ice-accelerations and loads is also beneficial for DP and position mooring in sea-ice infested waters. Due to the aggressive nature of the ice loads [10], control systems must be provided with more information to compensate for the higher dynamics of ice loads [11]. The drift of sea-ice can lead to the accumulation of ice rubble along the hull of the vessel [12], which can endanger stationkeeping operations. The problem is to detect local ice-induced accelerations without the need of installing strain gauges in the hull of the vessel.

This paper proposes to measure and to use locally induced vibrations in the ship's hull in order to evaluate the environment around the vessel. A distributed motion sensor setup for both full scale and model scale measurements is presented. The placement of the sensors is discussed as well as a mathematical model for the measured accelerations derived. A full scale application on an icebreaker ship demonstrates, that distributed motion sensing can be used to track changes in the attacking ice

conditions. During a voyage in the ice-infested waters of the Arctic, data was collected under different ice conditions and in open water from four spatially distributed IMUs placed on the Swedish icebreaker Oden. It is shown that the recorded local vibrations follow a t-distribution when the ship is affected by ice, but follow a normal distribution when the ship operates in open waters. Different test scenarios show that the parameters of the underlying t-distribution depend on the properties of the attacking ice and the state of ice encounter, e.g. the impact velocity. The properties of the ice around the vessel were extracted from a camera system. It is further shown that, due to the spatial distribution of the sensors, a local awareness of the ice conditions can be achieved (e.g. differences in ice conditions between the port and starboard side of the vessel). In a second application, a model scale experiment is conducted, which demonstrates that locally induced motions can be used to detect the angle of attack from waves in open water by calculating the phase difference of locally measured heave accelerations at different positions of the ship.

The scope of the paper is as follows: In section II a mathematical model describing the locally measured accelerations is given and the placement of the sensors is discussed. Section III presents the full scale application of distributed motion sensing on an icebreaker vessel. The experiment setup is described and 13 different test scenarios with different ice conditions are presented. The statistical characteristics of acceleration data from four IMU sensors is determined. For each scenario a camera system provides information about the ice conditions around the vessel. The changes in the statistical properties in each scenario and for each sensor is discussed and compared to the recorded ice conditions. Section IV presents the model scale application for angle of attack detection of incoming waves with the help of distributed motion sensing. The experiment setup is described and a mathematical model that includes locally induced wave motions is presented. A method is presented to estimate the angle of attack from incoming waves. Section V concludes this paper in a summary of the potential of distributed motion sensing and an outlook on upcoming work.

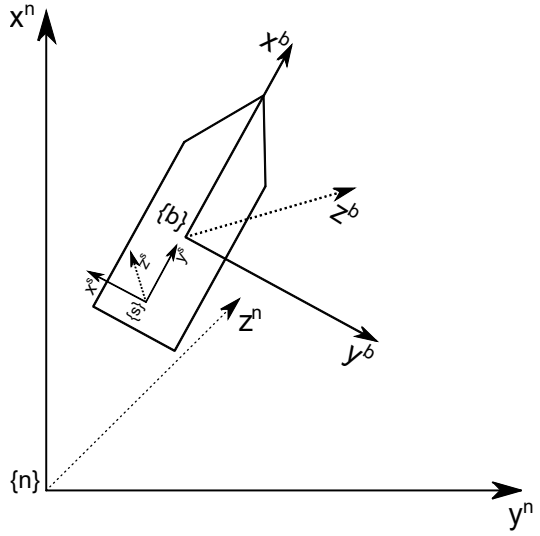

Fig. 1. Coordinate system definitions

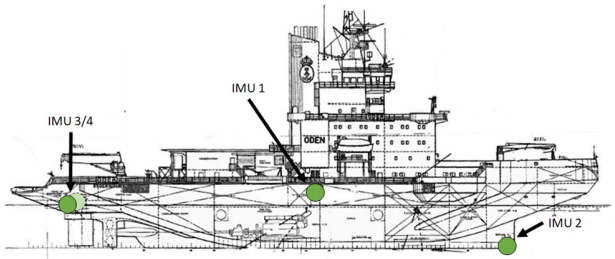

Fig. 2. Position of IMU sensors for ice induced vibration measurements

II. Distributed Motion Sensing

An IMU contains six sensors, out of which three orthogonal accelerometers measure the proper acceleration acting on the object the IMU is mounted on. Three orthogonal gyroscopes measure the angular rate. The readings from the gyroscopes are neglected in this work. As shown in Fig. 1, three coordinate systems have to be distinguished [13]: The North-East-Down (NED) coordinate system, denoted with the superscript {n}, is defined relative to the Earth's reference ellipsoid and assumed as an inertial reference frame [13]. The body-fixed reference frame, denoted with superscript {b}, is a moving coordinate frame fixed to a point of origin in the vessel. The sensor-fixed reference frame for each sensor, denoted with the superscript $\{s_i\}$, is the coordinate system fixed to the sensor i in the sensor mounting point. In this paper all sensor readings are aligned with the body frame of the vessel. The sensor output of the i^{th} IMU's three orthogonal accelerometers in the body reference frame can be combined in a vector $\boldsymbol{a}^b_{m,i} \in \mathbb{R}^3$. The sensor output is modelled, following [6] and [13],

$$\boldsymbol{a}^b_{m,i} = \boldsymbol{a}^b_{l,i} + \boldsymbol{R}^b_n(\boldsymbol{\Theta}_{nb})\boldsymbol{g}^n + \boldsymbol{b}^b + \boldsymbol{w}^b \tag{1}$$

with $\boldsymbol{a}^b_{l,i} \in \mathbb{R}^3$ representing the linear dynamic accelerations in the mounting point of sensor i, $\boldsymbol{R}^b_n(\boldsymbol{\Theta}_{nb})$ the rotation matrix between the NED frame and the body frame, which depends on the Euler angles $\boldsymbol{\Theta}_{nb} = (\phi, \theta, \psi)$, see also [13], $\boldsymbol{g}^n = (0,0,g)$ contains the gravity expressed in the NED frame, $\boldsymbol{b}^b \in \mathbb{R}^3$ contains the sensor biases and $\boldsymbol{w}^b \in \mathbb{R}^3$ accounts for the sensor noise of each accelerometer. Following [7], the linear dynamic acceleration in the vessel origin (VO), $\boldsymbol{a}^b_{vo} \in \mathbb{R}^3$, can be derived by taking into account the centrifugal, Coriolis, and Euler acceleration. Additionally, also local accelerations denoted $\boldsymbol{a}^b_{vib}$, which are not affecting the movement of the vessel, are taken into account by

$$\begin{aligned}\boldsymbol{a}^b_{vo} + \boldsymbol{a}^b_{vib} = \boldsymbol{a}^b_{l,i} - \boldsymbol{\alpha}^b \times \boldsymbol{l} - \boldsymbol{\omega}^b \times \boldsymbol{v}^b \\ - \boldsymbol{\omega}^b \times (\boldsymbol{\omega}^b \times \boldsymbol{l})\end{aligned} \tag{2}$$

where $\boldsymbol{\alpha} \in \mathbb{R}^3$ is the angular acceleration, $\boldsymbol{\omega}^b \in \mathbb{R}^3$ is the angular rate, and $\boldsymbol{l} \in \mathbb{R}^3$ is the lever arm between the center of the sensor's coordinate frame and the VO, see [7] for more details.

Accelerations caused by the hydrodynamics of the ship, by environmental action such as wind, waves, or sea-ice, and accelerations by the thrusters and propellers contribute to the linear dynamic accelerations in the VO. The additional locally measureable vibrations can either be caused by engine induced vibrations or by external effects. One of these external effects can be the interaction of the ship's hull with surrounding sea-ice.

The ship-ice interaction occurs generally in four steps: Breaking of the ice, rotation of the broken ice pieces, sliding against the hull, and clearing of the ice pieces [15]–[17]. Especially due to the crushing of ice and due to the sliding of the ice fragments along the hull, vibrations are induced that are locally measureable [8], [18].

Since the ship's structure damps the locally induced vibrations, the placement of the sensors is crucial to be able to capture them. The sensors must be placed as close as possible to the sources of the local vibrations. In the case of the interaction with sea-ice, this would be close to the ice-interaction zone inside the hull of the vessel. An example of the sensor placements is given in Fig. 2 and further discussed in the first application example.

III. Statistical Properties of Ice Induced Vibrations

During a six week expedition in the Arctic Ocean, data from four IMU sensors, distributed over the vessel, were collected while travelling in different ice conditions and in open water. Due to the placement of some sensors close to the ice-interaction zone, locally ice-induced vibrations were measureable.

A. Probability distribution of ice-induced accelerations

If the locally measureable vibrations are influenced by the ship-ice interaction, the properties of the measured acceleration signals will change. The ice breaking process can be seen as a stochastic process. As soon as the ship-ice interaction is dominant, the stochastic process of ice breaking will influence the stochastic properties of the locally induced vibrations, which are measured by the IMUs. The locally measured vibrations $\boldsymbol{a}_{vib}^{b}$ are described as a continuous random variable and $\boldsymbol{f}_{\boldsymbol{a}_{vib}}(\mathbf{x})$ is the probability density function (PDF) of the locally induced accelerations. Noise signals are commonly assumed to be Gaussian distribution. Gaussian distributed data produces a straight line on probability paper plot. If the data, however, shows heavier tails, it follows another probability distribution [19]. Besides the Gaussian distribution, the recorded vibration data is tested against the univariate t-distribution, the Cauchy distribution and the Laplace distribution. These three distributions are heavy tail distributions [20]. The correct distribution is determined by inserting the recorded and filtered data into a probability plot. With the help of maximum-likelihood estimators, the four probability distributions are fitted to the data. The Kolmogorov-Smirnov test is used to exclude probability distributions that do not fit the data on a significance level of 5 %.

The univariate t-distribution depends on three parameters: The location parameter μ, the scale parameter S, and the shape parameter ν. With the Gamma function $\Gamma(z) = \int_0^\infty t^{z-1}e^{-1}dt$, the PDF of the univariate t-distribution is:

$$f(\mathrm{x};\mu,S,\nu) = \frac{\Gamma(0.5+0.5\nu)}{\mathrm{S}\cdot\Gamma(0.5\nu)\sqrt{\pi\nu}} \cdot\left[1+\frac{1}{\nu}\frac{(\mathrm{x}-\mu)^2}{S^2}\right]^{-\frac{\nu+1}{2}} \tag{3}$$

The shape parameter $\nu \in \mathbb{R}^{>0}$ defines the tail of the distribution. If $\nu \to \infty$, the tails vanish and the t-distribution approaches the normal distribution. A Gaussian distribution is assumed for $\nu > 30$. The smaller the shape parameter ν gets, the more distinct the tails of the distribution are. The variance for the t-distribution is defined for $\nu > 2$ by

$$Var(\mathrm{x}) = S^2\frac{\nu}{\nu-2} \tag{4}$$

The Cauchy distribution results for $\nu = 1$ [21].

The Laplace distribution is a double exponential distribution, defined by the location parameter ν and the scale parameter b:

$$f(\mathrm{x};\mu,b) = \frac{1}{2b}\exp\left(-\frac{|\mathrm{x}-\mu|}{b}\right) \tag{5}$$

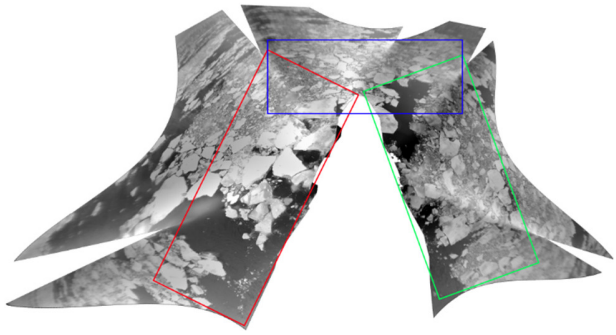

TABLE I.
TECHNICAL SPECIFICATION OF ACCELEROMETERS

Parameter	Value	Unit
Dynamic range	±5.25	g
Sensitivity	1.00	mg/LSB
Bias stability	0.1	mg
Velocity random walk	0.12	m/sec/hr$^{0.5}$
Output noise	5	mg rms

B. Experimental setup

During the SWEDARCTIC Arctic Ocean 2016 expedition [22], the Swedish icebreaker Oden was equipped with four IMU sensors according to Fig. 2. IMU 1 was placed in a central location of the vessel, close to the approximate center of gravity of the vessel. It is used as reference to measure global accelerations without the influence of locally induced accelerations. IMU 2 was placed close to the ice interaction zone, inside the ice-knife of the vessel and directly at the outer hull of the vessel. IMU 3 and IMU 4 were placed in the aft of the vessel on port (P) respectively starboard (SB) side. In contrast to IMU 2, the IMUs 3 and 4 could unfortunately not be placed directly on the outer hull due to safety regulations.

The sensors were of type ADIS 16364 from Analogue Devices. The technical specifications of the IMUs' accelerometers are given in TABLE I. Synchronization of data recording was guaranteed by a single-board computer (BeagleBone). Each BeagleBone was equipped with a highly precise real-time clock, which was synchronized via the network time protocol (NTP) to the ship's systems.

A camera system, which was also synchronized to the ship's systems, recorded the ice conditions around the vessel. After post-processing, a panorama image is obtained, which can be used to automatically determine the ice concentration and an indicator of the brokenness of the surrounding ice for each side of the vessel [23]. An example is shown in Fig. 3. Ahead, port, and the starboard part of the image are analyzed separately, according to the blue, red, and green marked areas in Fig. 3. The ice concentration is determined for each region by separating ice and water showing pixels. The brokenness is determined by edge detection and counting the edge pixels between two ice floes or between water and an ice floe. More information on how to obtain the ice conditions from the recorded images can be found in [23].

C. *Processing of recorded acceleration data*

The data from the accelerometers is processed in order to align all sensor readings to the body frame, remove the influence of the slowly varying biases, and to filter out noise. The processing steps are shown in Fig. 4.

D. *Scenarios*

For 13 different scenarios with different ice conditions and vessel speeds, the ice induced vibrations were analyzed by fitting four different probability distributions to 30 seconds of data of the three accelerometers of each IMU sensor. The time window of 30 seconds has been chosen to capture enough dynamics to model the tails of the distributions but still to be short enough to assume constant heading, speed, and wind influence. An overview of the scenarios and the recorded shipdata is given in TABLE III while the ice conditions are summarized in TABLE II.

Scenarios 1-3 are taken while the ship was travelling in open waters. In scenario 3, the ship gets close, but not in contact, with a major ice floe on starboard. In scenarios 4-6, the ship travelled through open ice with speeds of ~9.5 m/s for scenarios 4 and 5 and 1.2 m/s for scenario 6. In scenarios 7-11, the ship travelled slowly through close and very close pack-ice. In scenarios 12 and 13, the ship was standing still, with major, unbroken ice

TABLE III.
SHIPDATA DURING EACH ANALYZED SCENARIO

Scenario	Date and Time	SOG (m/s)	Heading (°)	True wind-speed (m/s)	True wind direction (°)
1	06.09.16 12:47	6.1	246.8	10.0	345.7
2	16.09.16 18:05	6.1	246.8	10.0	345.7
3	01.09.16 18:44	6.4	314.8	14.4	319.7
4	09.09.16 13:49	9.5	232.9	7.4	245.6
5	16.09.16 17:34	9.5	232.9	7.4	245.6
6	16.09.16 17:37	1.2	214.4	8.1	247.8
7	06.09.16 13:47	5.5	2.2	11.6	333.0
8	09.09.16 14:20	6.7	230.5	8.2	260.2
9	09.09.16 14:01	6.7	231.5	7.5	247.5
10	09.09.16 14:04	3.3	231.5	8.3	244.8
11	09.09.16 14:48	1.2	214.4	8.1	247.8
12	14.09.16 9:40	0.1	72.4	5.0	152.1
13	21.08.16 0:16	0.2	133.6	6.5	69.3

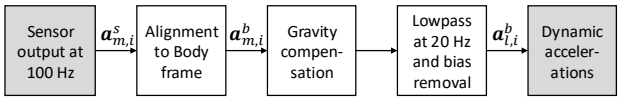

Fig. 4. Processing of sensor readings for each IMU

TABLE II.
RESULT FROM CAMERA IMAGE ANALYSIS

Scenario	Ice state	Water pixels in %			Brokenness of ice[a]		
		Ahead	*Port*	*SB*	*Ahead*	*Port*	*SB*
1	Open water	84.23	96.54	62.23	-	-	-
2	Open water	48.73	70.35	65.64	-	-	-
3	Open water, level ice SB	22.39	61.81	3.89	-	-	0.28
4	Open ice	26.69	7.32	25.01	4.21	10.39	7.84
5	Open ice	13.03	27.12	36.17	20.84	29.76	21.55
6	Open ice	43.98	14.15	43.99	10.30	22.19	10.57
7	Close pack-ice	19.09	8.63	18.40	1.94	7.65	0.95
8	Very close pack-ice	2.08	0.26	3.28	1.02	1.34	4.05
9	Very close pack-ice	11.47	2.27	6.63	1.44	1.34	0.83
10	Very close pack-ice	3.12	0.34	5.85	0.48	0.65	2.87
11	Very close pack-ice	2.97	0.88	15.09	1.68	3.91	5.68
12	Level ice at both sides	8.14	4.61	10.80	0.93	2.45	0.28
13	Level ice ahead	19.27	42.92	48.27	0.46	5.43	4.51

[a] Brokenness is an index describing the amount of broken ice in an image. 100 means that every ice showing pixel in the image shows broken ice, 0 means that no ice pixel shows broken ice.

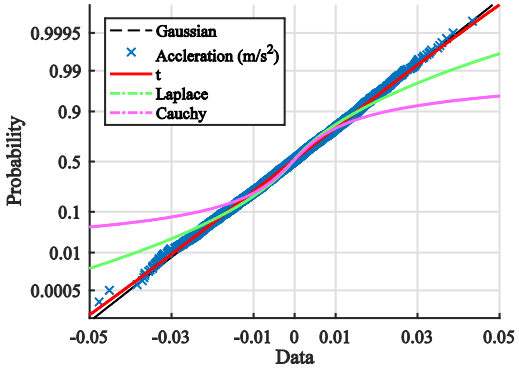

Fig. 5. Probability plot in open water of IMU 3 surge

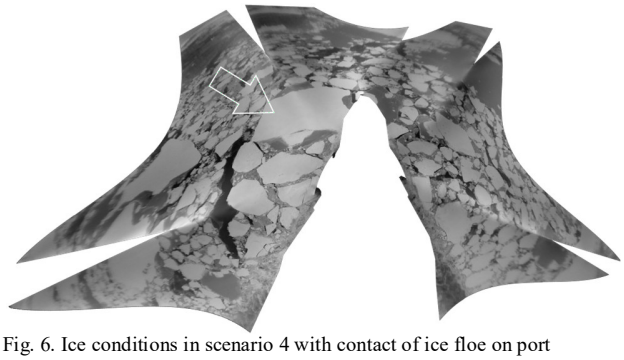
Fig. 6. Ice conditions in scenario 4 with contact of ice floe on port

TABLE IV.
P-VALUES FOR DIFFERENT DISTRIBUTIONS OF ACCELERATION DATA IN OPEN WATER (SCENARIOS 1-3)

Scenario / IMU	Gaussian			t (degrees of freedom in brackets)						Laplace			Cauchy		
	surge	*sway*	*heave*	*surge*		*sway*		*heave*		*surge*	*sway*	*heave*	*surge*	*sway*	*heave*
1 / IMU1	0.140	0.105	0.223	0.140	820193.046	0.104	1742718.967	0.222	2492868.710	0.000	0.000	0.000	0.000	0.000	0.000
1 / IMU2	0.834	0.158	0.001	0.910	25.330	0.251	26.290	0.511	6.557	0.000	0.000	0.000	0.000	0.000	0.000
1 / IMU3	0.782	0.061	0.423	0.782	1660634.014	0.296	21.040	0.423	1253873.622	0.000	0.000	0.000	0.000	0.000	0.000
1 / IMU4	0.370	0.562	0.986	0.372	3896261.261	0.577	100.545	0.914	53.158	0.000	0.000	0.000	0.000	0.000	0.000
2 / IMU1	0.719	0.778	0.883	0.721	1399657.179	0.776	878468.061	0.971	50.764	0.000	0.000	0.000	0.000	0.000	0.000
2 / IMU2	0.488	0.009	0.000	0.820	33.229	0.009	4079531.376	0.000	6017145.159	0.000	0.000	0.000	0.000	0.000	0.000
2 / IMU3[a]	0.750	0.967	0.310	0.846	140.040	0.907	99.100	0.310	2300228.744	0.000	0.000	0.000	0.000	0.000	0.000
2 / IMU4	0.927	0.666	0.426	0.927	2524694.046	0.667	2956476.760	0.000	4496663.239	0.000	0.000	0.000	0.000	0.000	0.000
3 / IMU1	0.701	0.255	0.756	0.703	305538.649	0.240	158.912	0.893	33.332	0.000	0.000	0.000	0.000	0.000	0.000
3 / IMU2	0.461	0.431	0.455	0.889	11.785	0.925	16.443	0.689	25.386	0.000	0.000	0.000	0.000	0.000	0.000
3 / IMU3	0.997	0.586	0.607	0.999	142.226	0.711	29.503	0.606	1775816.718	0.000	0.000	0.000	0.000	0.000	0.000
3 / IMU4	0.703	0.502	0.282	0.936	42.262	0.356	17.823	0.281	3608822.858	0.000	0.000	0.000	0.000	0.000	0.000

[a]See Fig. 5 for a probability plot example

TABLE V.
P-VALUES FOR DIFFERENT DISTRIBUTIONS OF ACCELERATION DATA IN OPEN ICE (SCENARIOS 4-6)

Scenario / IMU	Gaussian			t (degrees of freedom in brackets)						Laplace			Cauchy		
	surge	*sway*	*heave*	*surge*		*sway*		*heave*		*surge*	*sway*	*heave*	*surge*	*sway*	*heave*
4 / IMU1	0.940	0.759	0.843	0.960	71.893	0.845	27.094	0.885	41.269	0.000	0.000	0.000	0.000	0.000	0.000
4 / IMU2	0.000	0.001	0.000	0.779	5.792	0.575	6.157	0.878	4.225	0.009	0.000	0.108	0.000	0.000	0.000
4 / IMU3	0.637	0.069	0.812	0.964	15.793	0.302	8.882	0.910	60.480	0.000	0.000	0.000	0.000	0.000	0.000
4 / IMU4	0.426	0.098	0.603	0.403	17.048	0.153	11.791	0.635	362.809	0.000	0.000	0.000	0.000	0.000	0.000
5 / IMU1	0.364	0.082	0.958	0.364	2959770.773	0.082	4022347.152	0.959	2177582.861	0.000	0.000	0.000	0.000	0.000	0.000
5 / IMU2	0.000	0.161	0.000	0.192	4.727	0.180	10.764	0.000	64.511	0.000	0.000	0.000	0.000	0.000	0.000
5 / IMU3	0.571	0.415	0.935	0.908	26.535	0.481	34.298	0.989	62.035	0.000	0.000	0.000	0.000	0.000	0.000
5 / IMU4	0.645	0.647	0.253	0.644	3788174.650	0.648	1176429.805	0.256	1095565.369	0.000	0.000	0.000	0.000	0.000	0.000
6 / IMU1	0.215	0.000	0.103	0.230	137.670	0.014	7.791	0.103	3637209.864	0.000	0.000	0.000	0.000	0.000	0.000
6 / IMU2	0.000	0.000	0.000	0.000	2.501	0.000	3.247	0.000	27.742	0.000	0.000	0.000	0.000	0.000	0.000
6 / IMU3	0.893	0.134	0.982	0.934	208.654	0.135	4510293.111	0.992	156.398	0.000	0.000	0.000	0.000	0.000	0.000
6 / IMU4	0.003	0.204	0.118	0.245	10.247	0.205	1602917.111	0.425	7.547	0.000	0.000	0.000	0.000	0.000	0.000

TABLE VI.
P-VALUES FOR DIFFERENT DISTRIBUTIONS OF ACCELERATION DATA IN CLOSE AND VERY CLOSE ICE (SCENARIOS 7-13)

7/ IMU1	0.371	0.035	0.874	0.476	77.312	0.035	1503465.676	0.857	395.886	0.000	0.000	0.000	0.000	0.000	0.000
7 / IMU2	0.000	0.000	0.000	0.968	5.209	0.647	4.182	0.391	3.384	0.002	0.012	0.016	0.000	0.000	0.000
7 / IMU3	0.005	0.458	0.724	0.614	7.106	0.653	14.130	0.779	129.300	0.003	0.000	0.000	0.000	0.000	0.000
7 / IMU4	0.000	0.002	0.172	0.847	5.798	0.879	8.041	0.683	14.045	0.000	0.001	0.000	0.000	0.000	0.000
8 / IMU1	0.676	0.774	0.271	0.595	49.320	0.774	2900316.526	0.270	1327104.681	0.000	0.000	0.000	0.000	0.000	0.000
8 / IMU2	0.000	0.000	0.000	0.800	3.624	0.441	4.239	0.879	3.976	0.092	0.005	0.013	0.000	0.000	0.000
8 / IMU3	0.005	0.000	0.267	0.790	6.486	0.291	5.093	0.584	11.010	0.002	0.000	0.000	0.000	0.000	0.000
8 / IMU4	0.000	0.002	0.026	0.539	6.253	0.084	8.321	0.153	11.620	0.000	0.000	0.000	0.000	0.000	0.000
9 / IMU1	0.478	0.685	0.517	0.477	3581935.297	0.686	1684267.334	0.341	32.464	0.000	0.000	0.000	0.000	0.000	0.000
9 / IMU2	0.000	0.000	0.000	0.008	3.906	0.129	4.850	0.507	3.144	0.004	0.000	0.127	0.000	0.000	0.000
9 / IMU3	0.225	0.932	0.065	0.799	18.322	0.967	88.690	0.572	9.594	0.000	0.000	0.000	0.000	0.000	0.000
9 / IMU4	0.122	0.098	0.002	0.995	10.919	0.120	141.652	0.659	6.386	0.000	0.000	0.000	0.000	0.000	0.000
10 / IMU1	0.516	0.210	0.442	0.867	22.162	0.210	4223793.302	0.639	62.955	0.000	0.000	0.000	0.000	0.000	0.000
10 / IMU2	0.000	0.005	0.000	0.539	5.251	0.063	16.770	0.835	5.806	0.001	0.000	0.011	0.000	0.000	0.000
10 / IMU3	0.018	0.000	0.004	0.638	7.803	0.673	5.099	0.395	6.590	0.000	0.000	0.000	0.000	0.000	0.000
10 / IMU4	0.023	0.421	0.354	0.986	8.492	0.669	16.455	0.496	13.125	0.000	0.000	0.000	0.000	0.000	0.000
11 / IMU1	0.691	0.000	0.452	0.691	3128931.064	0.000	14.175	0.452	515611.289	0.000	0.000	0.000	0.000	0.000	0.000
11 / IMU2	0.000	0.000	0.000	0.021	2.296	0.000	2.625	0.056	1.728	0.000	0.000	0.000	0.000	0.000	0.009
11 / IMU3[b]	0.000	0.000	0.000	0.962	3.126	0.256	2.795	0.935	2.783	0.045	0.008	0.198	0.000	0.000	0.000
11 / IMU4	0.000	0.000	0.000	0.367	4.306	0.021	8.219	0.566	4.735	0.005	0.000	0.002	0.000	0.000	0.000
12 / IMU1	0.982	0.893	0.106	0.981	3855881.438	0.972	80.300	0.106	984353.806	0.000	0.000	0.000	0.000	0.000	0.000
12 / IMU2	0.371	0.145	0.000	0.821	11.328	0.288	9.453	0.182	6.653	0.000	0.000	0.000	0.000	0.000	0.000
12 / IMU3	0.000	0.000	0.000	0.294	2.781	0.087	3.450	0.012	3.859	0.004	0.000	0.000	0.000	0.000	0.000
12 / IMU4	0.322	0.862	0.198	0.816	10.359	0.838	42.967	0.413	10.659	0.000	0.000	0.000	0.000	0.000	0.000
13 / IMU1	0.586	0.907	0.712	0.588	3296372.495	0.850	22.686	0.712	1102895.316	0.000	0.000	0.000	0.000	0.000	0.000
13 / IMU2	0.219	0.181	0.000	0.567	11.681	0.494	14.028	0.338	4.768	0.000	0.000	0.001	0.000	0.000	0.000
13 / IMU3	0.000	0.000	0.000	0.578	3.190	0.433	2.549	0.339	3.054	0.002	0.002	0.002	0.000	0.000	0.000
13 / IMU4	0.733	0.515	0.133	0.961	23.886	0.530	211.617	0.218	22.873	0.000	0.000	0.000	0.000	0.000	0.000

[b]See Fig. 7 for a probability plot example

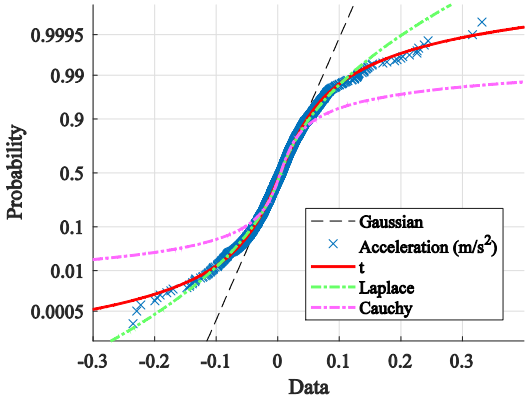

Fig. 7. Probability plot in very close ice of IMU 3 surge

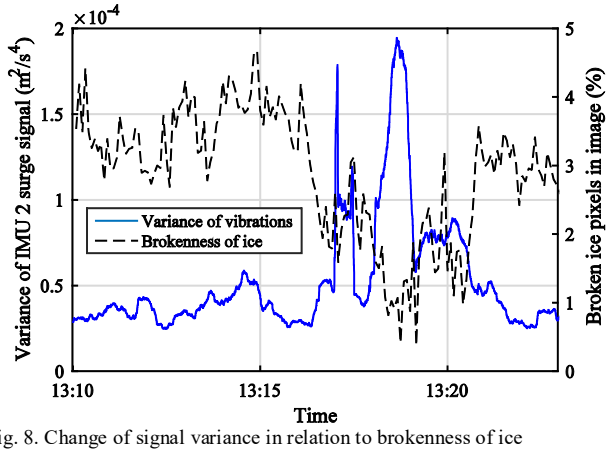

Fig. 8. Change of signal variance in relation to brokenness of ice

floes on both starboard and port side or, as in scenario 13, the bow of the ship was, before the measurement, rammed into an ice floe.

E. Sstatistical characteristics of ice-induced vibrations

a) Ship travelling in open waters: When the ship travels in open waters, ice-induced accelerations are not present. As shown in TABLE IV, the acceleration data from all four IMUs, except the heave acceleration data from IMU 2 in the bow of the vessel, follow Gaussian distributions. Outliers in the data from IMU 2, as a result from slamming of the vessel's bow, cause heavier tails in the data. It is noticeable, that in those cases the underlying t-distribution has a high number of degrees of freedoms, which makes it close to a Gaussian distribution. In cases of very high degrees of freedom, the iterative solver of the maximum likelihood estimator could not converge. Both the Laplace and Cauchy distributions are unsuitable for describing the data, since no or only weak tails are present in open water acceleration data.

b) Ship travelling in open ice: TABLE V shows the result from distribution fitting for recorded acceleration data in open ice. Some of the recorded data shows such distinct outliers, that the tail of the data can be best captured with a t-distribution. In scenario 4, the data shows distinct outliers in the bow (IMU 2) and port (IMU 3) sensors' data, however not in the starboard (IMU 4) sensor data. The reason is a direct contact of the ship's hull with a bigger unbroken ice floe on the portside of the bow of the vessel, as it can be seen in Fig. 6. Again, both the Laplace and Cauchy distribution are unsuitable for describing the data.

c) Ship travelling in close or very close ice: Except for IMU 1 and some single cases, the Gaussian distribution is unsuitable to describe the acceleration data captured when the ship travels in close or very close ice. IMU 1 is an exception, because it was mounted mid-ships, far away from the hull and is thus not capable of capturing the ice-induced vibrations. In general the t-distribution is the best choice to describe the statistical behaviour of the ice-induced accelerations. It is also noticeable, that the degrees of freedom of the t-distribution decreased compared to the open ice scenarios 4-6. The reason are more distinct outliers, caused by sudden interaction of ice

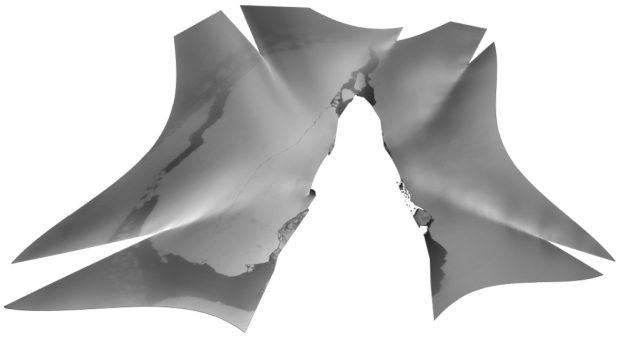

Fig. 9. Ice conditions in scenario 12 stationkeeping in level ice

with the ship's hull. An example of the distinct tails of the data can be seen in Fig. 7. In Fig. 8, the change of the signal variance in relation to the ice conditions for a continous measurement is shown. The variance of the t-distribution is given in (4) and depends on both the degrees of freedom ν and the scale of the distribution S. Recursively, the t-distribution parameters were estimated with a window length of 30 seconds over a time of 12 minutes for the surge acceleration data from IMU 2 (15th September 2016). The ship was travelling in a field of ice floes of about 20-30 meters diameter at a speed of 5-6 m/s. The variance was calculated and plotted together with the ice brokenness index from the camera images. At 13:17 the ship encountered a larger, unbroken ice floe. This results in a significant increase of variance, which can be seen as an indicator of a higher energy exchange between the ship and the surounding ice.

d) Ship standing still in close ice: The two scenarios 12 and 13 were recorded when the ship was stationkeeping in level ice, as shown in Fig. 9. IMU 1 is again not capable to capture local dynamics, which is why the data is normal distributed. IMUs 2-4 are located closer to the hull record vibrations, which allow them to capture the heavier tail t-distributed hull vibrations. This means that also during stationkeeping, ice-induced vibrations, probably caused by the ice drift, is noticeable by the accelerometers.

IV. Model scale experiment to detect angle of attack of incoming waves

A. Experimental setup

Experiments were performed with a 1:90 scaled C/S Inoccean Cat I Drillship (CSAD, short for Cybership Arctic Drillship), a model of the CAT I Drillship [24]. A setup of four spatially distributed motion sensors were mounted inside the hull, as illustrated in Fig. 10. The ADIS16364 was used in the experiments, with each IMU connected to an Arduino Leonardo™ ETH microcontroller. One microcontroller was set to be the leader, and the three other operated as followers. Time-synchronization was achieved with an interrupt signal from the leader to the followers at a pre-defined frequency. Measured acceleration data were sent over an Ethernet interface and collected on a cRIO™ platform. Due to computational limitations of the cRIO™, the sampling rate was set to 20 Hz.

Experiments were carried out in the basin of the Marine Cybernetics Laboratory (MC-Lab) at NTNU. The position and heading of the vessel were fixed as illustrated in Fig. 11. In Fig. 12 a photo of the ship model in the basin with the experimental setup is shown. The fixation works as a stiff DP-setup with nearly free motions in heave, roll and pitch, and limited, but not constrained, motions in surge, sway and yaw. In total seven experiments were carried out, with heading fixed to $0°, 30°, 60°, 90°, 120°, 150°$, and $180°$. Stoke's 1st order waves excited the vessel, with a wave period of 1.5 seconds. Due to some temporary modifications in the basin, the wave beach was not working properly and the waves were strongly reflected. As a result, each experiment was only performed for 50 seconds because the reflected waves affected the wave spectrum and direction of incoming waves.

B. Modeling

A new reference frame is introduced for the model experiments, which is a basin fixed reference frame denoted {f}. This reference frame is assumed an inertial reference frame for navigation in the basin, similar to NED.

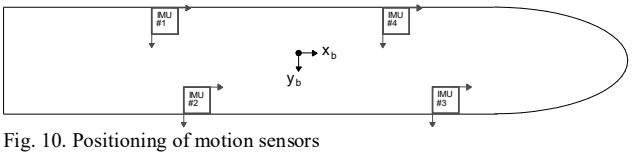

Fig. 10. Positioning of motion sensors

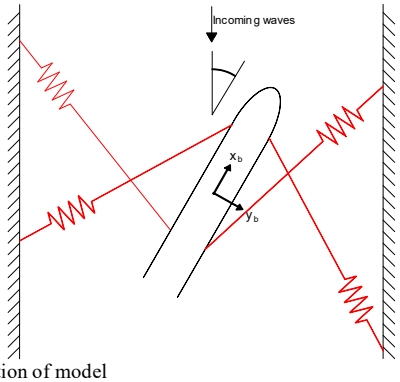

Fig. 11. Fixation of model

Fig. 12. Photo of CSAD with experimental setup

Due to spatial limitations, each sensor frame is rotated to be parallel with the body frame using a rotation matrix. Based on measured Euler angle offset, the body-parallel accelerations were calculated as

$$\boldsymbol{a}^b_{m,i} = \boldsymbol{R}^b_s(\boldsymbol{\Theta}'_{bsi})\boldsymbol{a}^s_{m,i} \tag{6}$$

where $\boldsymbol{a}^b_{m,i} \in \mathbb{R}^3$ is the linear accelerations of sensor i rotated to {b}, $\boldsymbol{\Theta}'_{bsi} \in \mathbb{R}^3$ is the initial angle offset of sensor frame i relative to {b}, and $\boldsymbol{a}^s_{m,i} \in \mathbb{R}^3$ is the measured accelerations of sensor i. In contrast to the full-scale experiments, the gravity was modeled as unknown using the differential equation

$$\dot{\boldsymbol{g}} = -\boldsymbol{\omega} \times \boldsymbol{g}, \tag{7}$$

where $\boldsymbol{g} \in \mathbb{R}^3$ is the gravity vector and $\boldsymbol{\omega} \in \mathbb{R}^3$ is the angular rate of the vessel. Using the method of [25], the kinematic model is

$$\begin{aligned} \dot{\boldsymbol{p}}^{s,i}_{s/f} &= -\boldsymbol{\omega} \times \boldsymbol{p}^{s,i}_{s,i/f} - \boldsymbol{v}^{s,i}_{s,i/f} \\ \dot{\boldsymbol{v}}^{s,i}_{s,i/f} &= -\boldsymbol{\omega} \times \boldsymbol{v}^{s,i}_{s,i/f} - \boldsymbol{g} - \boldsymbol{b} + \boldsymbol{a}^b_{m,i} \\ \dot{\boldsymbol{g}} &= -\boldsymbol{\omega} \times \boldsymbol{g} \\ \dot{\boldsymbol{b}} &= \boldsymbol{0} \end{aligned} \tag{8}$$

where $\boldsymbol{p}^{si}_{si/f} \in \mathbb{R}^3$ is the position of sensor i in the basin frame, $\boldsymbol{v}^{si}_{si/f} \in \mathbb{R}^3$ is the linear velocity of the sensor, and $\boldsymbol{b} \in \mathbb{R}^3$ is the sensor bias modeled as a random walk. The kinematic model was modeled as an LTV system, and solved using the discrete time Kalman Filter. The measurement of the state in the Kalman Filter, $y = \boldsymbol{p}^{si}_{si/f}$, was the measured position from the camera based positioning system in MC-Lab.

The waves are modeled with the assumption of deep water, which gives the dispersion relation $k = \omega^2/g$, where k is the wave number, ω is the circular frequency of the waves, and g is the gravity constant. The phase velocity may now be expressed in terms of the wave period calculated by

$$c = \frac{g}{2\pi}T \tag{9}$$

where $c \in \mathbb{R}$ is the phase velocity of the waves, and $T \in \mathbb{R}$ is the wave period.

C. Estimating angle of attack of incoming waves

The proposed method for estimating the direction of incoming waves is based on the idea that the system of distributed motion sensors can measure the wave force field as the waves travel through the hull. By measuring the point in time of extrema in heave acceleration in each sensor, one can estimate the direction of incoming waves. Using the phase velocity of the waves and the distance between the sensors, one

can calculate the time it will take for the waves to travel between the sensors. For example, setting sensor #1 as the reference sensor, the distance between sensor #1 and #4 in the x-y plan is given as $\|\boldsymbol{p}_{s1/s4}^{s1}\|$ when sensor #4 is projected onto the x-y plane of sensor #1. The time it takes for the wave peak to travel from sensor #1 to #4 is now estimated as a function of the direction of incoming waves, β, given as

$$t_e(\beta) = \frac{\|\boldsymbol{p}_{s1/s4}^{s1}\|\cos(-\beta)}{c} \tag{10}$$

where $\beta \in \mathbb{R}$ is the angle of attack of the incoming waves, expressed in $\{s_1\}$. It should be noted that this method defines the time difference such that negative time means the peak occurred in sensor #4 before #1. In addition, as the estimated angle of attack is given in {b}, a positive heading in the basin corresponds to an equal negative angle of attack in {b}. Further, as waves travel through the hull, the measured time difference, t_m, in peaks in heave acceleration for both sensors is used to estimate β. This is solved as an optimization problem

$$\min_{\beta \in [-180,\ 180]} t_e(\beta) - t_m \tag{11}$$

By augmenting this method to include all four sensors, one gets a unique time difference for all directions of incoming waves. The objective of minimizing the time difference then becomes an optimization problem in the least squares sense.

D. Signal processing

The algorithm for estimating the angle of attack of incoming waves was implemented as an online algorithm on the vessel. Hence, to avoid time delay, there was no noise filtering except the Kalman Filter.

E. Results

The time series presented in Fig. 13 are the first 50 seconds when waves hit the vessel, with heading fixed to 0°. When calculating $t_e(\beta)$, the estimated angle of incoming waves is modeled with step size of 10°. The estimates are assumed to be Gaussian distributed when calculating the variance and standard deviation. The mean value of the estimated angles is annotated in the figure, together with the standard deviation. The estimates have a large variance, while the mean value is close to the true direction.

The mean estimate and standard deviation for all headings are presented in Fig. 14, with values given in the legend. The polar plot illustrates estimated direction of incoming waves expressed in {b}. The method performs well for all headings, with a maximum discrepancy of 12°. The standard deviation varies more, where head and beam sea have a larger variance compared to headings between 30° and 120°.

In Fig. 15 the performance of the online algorithm for finding the acceleration extrema is investigated. The figure shows the heave acceleration of all motion sensors for the first 10 seconds when the wave train hits the vessel. The illustrated experiment is with heading fixed to 0°. The local maximum and minimum values for all sensors are marked with circles and squares. It is clear that the extrema found are affected by noise, as the measured value is affected by measurement noise. The figure also illustrates how the wave travel through the hull, as there is a clear and consistent delay from peak in heave acceleration from the two sensors in the bow to the two located aft.

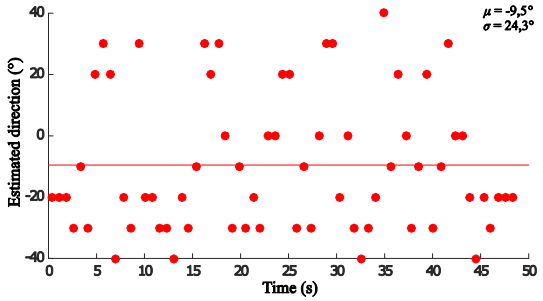

Fig. 13. Estimated angle of attack of inc. waves with heading fixed to 0°

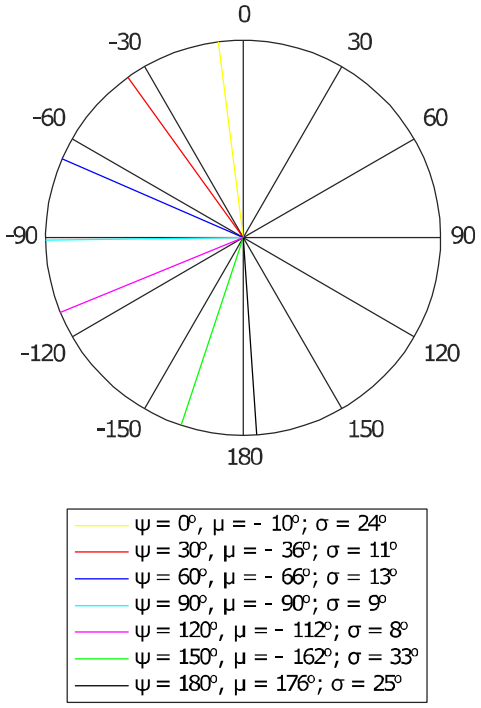

Fig. 14. Estimated angle of attack of incoming waves for all headings

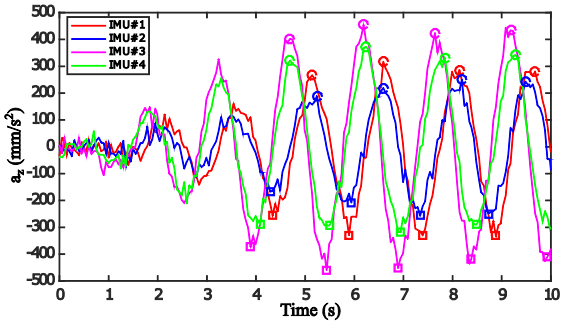

Fig. 15. Point in time of extrema in heave acceleration for all four sensors

V. Conlusion

This paper presented a method to measure and use locally induced accelerations on marine vessels. By placing accelerations sensors not in the center of the vessel, but instead close to the hull of the vessel, the sensors are able to record locally induced accelerations, that origin from the environment around the vessel. In two applications the advantages of the distributed acceleration sensing approach are demonstrated. By measuring local accelerations in the hull of a full-scale icebreaker vessel and evaluating the statistical properties of the locally induced accelerations, a relationship can be found between the ice conditions around the vessel and the measured hull vibrations. In a second, model-scale application, it was shown that locally measured heave accelerations can be used to identify wave forces traveling through the hull. This can be used for identifying the direction of incoming waves, which can be useful for autonomous vessels.

Further work is required in developing the applications of distributed motion sensing on marine vessels. For ice-induced motion sensing, a system for drift detection around a stationkeeping vessel can be developed, which utilizes the changes in statistical properties of ice-induced vibrations presented in this paper. This drift estimate can be used as support for vessels, who are stationkeeping in ice. Ice-induced motion detection can also be developed further into a decision support system for ice-going vessels, warning the crew of dangerous ice conditions around a vessel travelling in ice. As shown in the second application, distributed motion sensing can be used for direction detection of incoming waves. This can be further used as input to heading controller for weather vaning vessels, which are in stationkeeping operations and compared to standard weather vaning methods.

Acknowledgment

The authors would like to thank the Research Council of Norway (RCN) for financial support through projects 203471 CRI SAMCoT and 223254 CoE AMOS. This work was supported by the Swedish Polar Research Secretariat as part of the research program SWEDARCTIC 2016.

References

[1] T. H. Bryne, J. M. Hansen, R. H. Rogne, N. Sokolova, T. I. Fossen, and T. A. Johansen, 'Nonlinear Observers for Integrated INS\/GNSS Navigation: Implementation Aspects', *IEEE Control Syst.*, vol. 37, no. 3, pp. 59–86, Jun. 2017.

[2] T. H. Bryne, 'Nonlinear Observer Design for Aided Inertial Navigation of Ships', Norwegian University of Science and Technology, 2017.

[3] T. H. Bryne, T. I. Fossen, and T. A. Johansen, 'Design of inertial navigation systems for marine craft with adaptive wave filtering aided by triple-redundant sensor packages', *Int. J. Adapt. Control Signal Process.*, no. 7491, pp. 522–544, 2015.

[4] R. Galeazzi *et al.*, 'Parametric roll resonance monitoring using signal-based detection', *Ocean Eng.*, vol. 109, pp. 355–371, Nov. 2015.

[5] M. Johnston, R. Frederking, G. Timco, and M. Miles, 'MOTAN: A Novel Approach for determining Ice-Induced Global Loads on Ships', *Proc. MARI-TECH 2003*, no. 5, pp. 1–17, 2003.

[6] M. Johnston, R. Frederking, G. Timco, and M. Miles, 'Using Motan To Measure Global Accelerations of the Ccgs Terry Fox During Bergy Bit Trials', *Int. Conf. Offshore Mech. Arct. Eng.*, pp. 1–8, 2004.

[7] O. K. Kjerstad and R. Skjetne, 'Disturbance Rejection by Acceleration Feedforward for Marine Surface Vessels', *IEEE Access*, vol. 4, pp. 2656–2669, 2016.

[8] M. Bjerkås, A. Skiple, and O. Iver Røe, 'Applications of continuous wavelet transforms on ice load signals', *Eng. Struct.*, vol. 29, no. 7, pp. 1450–1456, Jul. 2007.

[9] B. Leira, L. Børsheim, Ø. Espeland, and J. Amdahl, 'Ice-load estimation for a ship hull based on continuous response monitoring', *Proc. Inst. Mech. Eng. Part M J. Eng. Marit. Environ.*, vol. 223, no. 4, pp. 529–540, Nov. 2009.

[10] S. Kerkeni, X. D. Santo, and I. Metrikin, 'Dynamic Positioning in ice - Comparison of control laws in open water and ice', in *Proceedings of the ASME 2013 32nd International Conference on Ocean, Offshore and Arctic Engineering*, 2013.

[11] Ø. K. Kjerstad, I. Metrikin, S. Løset, and R. Skjetne, 'Experimental and phenomenological investigation of dynamic positioning in managed ice', *Cold Reg. Sci. Technol.*, vol. 111, pp. 67–79, Mar. 2015.

[12] S. Løset, K. N. Shkhinek, O. T. Gudmestad, and K. V Høyland, *Actions from ice on Arctic offshore and coastal structures*. 2006.

[13] T. I. Fossen, *Handbook of Marine Craft Hydrodynamics and Motion Control*. Chichester, UK: John Wiley & Sons, Ltd, 2011.

[14] P. Batista, C. Silvestre, and P. Oliveira, 'On the observability of linear motion quantities in navigation systems', *Syst. Control Lett.*, vol. 60, no. 2, pp. 101–110, 2011.

[15] K. Riska, 'Ship-ice interaction in ship design: Theory and practice', Eolss Publisher, 2011.

[16] R. Lubbad and S. Løset, 'A numerical model for real-time simulation of ship-ice interaction', *Cold Reg. Sci. Technol.*, vol. 65, no. 2, pp. 111–127, 2011.

[17] B. Su, K. Riska, and T. Moan, 'A numerical method for the prediction of ship performance in level ice', *Cold Reg. Sci. Technol.*, vol. 60, no. 3, pp. 177–188, 2010.

[18] D. S. Sodhi, 'Ice - Structure Interaction During Indentation Tests', in *Ice-Structure Interaction*, Berlin, Heidelberg: Springer Berlin Heidelberg, 1991, pp. 619–640.

[19] A. Willersrud, M. Blanke, L. Imsland, and A. Pavlov, 'Drillstring Washout Diagnosis Using Friction Estimation and Statistical Change Detection', *IEEE Trans. Control Syst. Technol.*, vol. 23, no. 5, pp. 1886–1900, 2015.

[20] N. L. Johnson, *Continuous univariate distributions Vol. 1*. New York: John Wiley & Sons Inc, 1994.

[21] C. Aeschliman, J. Park, and A. C. Kak, 'A novel parameter estimation algorithm for the multivariate t-distribution and its application to computer vision', *Lect. Notes Comput. Sci. (including Subser. Lect. Notes Artif. Intell. Lect. Notes Bioinformatics)*, vol. 6312 LNCS, no. PART 2, pp. 594–607, 2010.

[22] K. Gårdfeldt and Å. Lindgren, 'SWEDARCTIC Arctic Ocean 2016', Stockholm, 2017.

[23] H.-M. Heyn, M. Knoche, Q. Zhang, and R. Skjetne, 'A system for automated vision-based sea-ice concentration detection and floe-size distribution indication from an icebreaker', in *Proceedings of the 36th International Conference on Ocean, Offshore & Arctic Engineering*, 2017.

[24] J. Bjørnø, H.-M. Heyn, R. Skjetne, A. Dahl, and P. Frederich, 'Modeling, parameter identification and thruster-assisted position mooring of C/S Inocean CAT I Drillship', in *Proceedings of the 36th International Conference on Ocean, Offshore & Arctic Engineering*, 2017.

[25] P. Batista, C. Silvestre, P. Oliveira, and B. Cardeira, 'Accelerometer Calibration and Dynamic Bias and Gravity Estimation: Analysis, Design, and Experimental Evaluation', *IEEE Trans. Control Syst. Technol.*, vol. 19, no. 5, pp. 1128–1137, Sep. 2011.